Citation: CPT Pharmacometrics Syst. Pharmacol. (2019) 8, 489–499; doi:10.1002/psp4.12408

ARTICLE

Evaluation of the Drug–Drug Interaction Potential of Acalabrutinib and Its Active Metabolite, ACP-5862, Using a Physiologically-Based Pharmacokinetic Modeling Approach

Diansong Zhou[1,*], Terry Podoll[2,†], Yan Xu[2], Ganesh Moorthy[1], Karthick Vishwanathan[1], Joseph Ware[2], J. Greg Slatter[2,†] and Nidal Al-Huniti[1]

Acalabrutinib, a selective, covalent Bruton tyrosine kinase inhibitor, is a CYP3A substrate and weak CYP3A/CYP2C8 inhibitor. A physiologically-based pharmacokinetic (PBPK) model was developed for acalabrutinib and its active metabolite ACP-5862 to predict potential drug–drug interactions (DDIs). The model indicated acalabrutinib would not perpetrate a CYP2C8 or CYP3A DDI with the sensitive CYP substrates rosiglitazone or midazolam, respectively. The model reasonably predicted clinically observed acalabrutinib DDI with the CYP3A perpetrators itraconazole (4.80-fold vs. 5.21-fold observed) and rifampicin (0.21-fold vs. 0.23-fold observed). An increase of two to threefold acalabrutinib area under the curve was predicted for coadministration with moderate CYP3A inhibitors. When both the parent drug and active metabolite (total active components) were considered, the magnitude of the CYP3A DDI was much less significant. PBPK dosing recommendations for DDIs should consider the magnitude of the parent drug excursion, relative to safe parent drug exposures, along with the excursion of total active components to best enable safe and adequate pharmacodynamic coverage.

Study Highlights

WHAT IS THE CURRENT KNOWLEDGE ON THE TOPIC?
☑ Acalabrutinib, a Bruton tyrosine kinase inhibitor, received accelerated approval by the US Food and Drug Administration for the treatment of adult patients with mantle cell lymphoma who have received at least one prior therapy.

WHAT QUESTION DID THIS STUDY ADDRESS?
☑ Physiologically-based pharmacokinetic (PBPK) modeling predicted the effect of CYP3A modulators on the pharmacokinetics of acalabrutinib and its active metabolite ACP-5862. Acalabrutinib as victim or perpetrator of CYP enzymes was assessed to guide its appropriate dosing in clinical practice.

WHAT DOES THIS STUDY ADD TO OUR KNOWLEDGE?
☑ PBPK modeling recommended a dose of 100 mg once a day and 200 mg twice a day for use with a moderate CYP3A inhibitor or a strong CYP3A4 inducer, respectively. PBPK analysis shows that acalabrutinib has no clinically relevant effects on sensitive CYP3A4 or CYP2C8 substrates. CYP3A modulator effects on acalabrutinib pharmacokinetics may be less significant when a total active component is considered.

HOW MIGHT THIS CHANGE DRUG DISCOVERY, DEVELOPMENT, AND/OR THERAPEUTICS?
☑ PBPK models of drug interactions that incorporate the impact of exposure to active metabolites, when verified with suitable clinical trial results, may give more relevant estimates of drug–drug interaction magnitude and therefore afford dosing recommendations that ensure both safety and adequate pharmacodynamic coverage.

Bruton tyrosine kinase (BTK) is a key component of B-cell receptor signaling critical for cell proliferation, migration, and survival.[1–3] BTK inhibition results in antitumor activity in preclinical animal models as well as in clinical studies.[4] BTK knockdown induces tumor cell death in B-cell receptor signaling-dependent primary chronic lymphocytic leukemia (CLL) cells and lymphoma cell lines.[5,6] Acalabrutinib is a highly selective, potent, irreversible, covalent BTK inhibitor designed to minimize off-target activity when compared with ibrutinib.[7,8] Acalabrutinib (Calquence Acerta Pharma, South San Francisco, CA) received accelerated approval by the US Food and Drug Administration for the treatment of adult

[1]Quantitative Clinical Pharmacology, Early Clinical Development, IMED Biotech Unit, AstraZeneca, Boston, Massachusetts, USA; [2]DMPK/Clinical Pharmacology, Acerta Pharma, South San Francisco, California, USA. *Correspondence: Diansong Zhou (diansong.zhou@astrazeneca.com)
[†]Former employee.
Received: February 19, 2019; accepted: March 22, 2019. doi:10.1002/psp4.12408

patients with mantle cell lymphoma who have received at least one prior therapy.[9,10] Acalabrutinib is currently under development for other hematological malignancies, including CLL and diffuse large B-cell lymphoma.

Acalabrutinib and ibrutinib have similar biological profiles in primary CLL cells; however, acalabrutinib appears to have fewer off-target effects in healthy B lymphocytes than ibrutinib.[11–13] In a clinical study of patients with relapsed CLL, the overall response rate with acalabrutinib was 95% after a median follow-up of 14.3 months (range 0.5–20).[5] In a clinical study of patients with relapsed/refractory mantle cell lymphoma, the investigator-assessed overall response rate was 81% (95% confidence interval, 73–87%) after a median follow-up of 15.2 months (range 0.3–23.7).[14] Acalabrutinib exhibited a favorable safety profile in these studies.

Acalabrutinib is rapidly absorbed with a short oral half-life of about 1.57 hours in healthy subjects, with an absolute oral bioavailability of 25%.[15] The pharmacokinetics (PK) of acalabrutinib were generally linear in the 75–250 mg range in patients, and no accumulation of acalabrutinib was observed after multiple doses.[16] During clinical studies, ACP-5862 was identified as the major, and pharmacologically active, metabolite of acalabrutinib in plasma. ACP-5862 has ~ 50% potency for BTK inactivation relative to parent acalabrutinib and has a similar kinase selectivity profile.[9] These data indicate that ACP-5862 may also contribute to efficacy and safety after acalabrutinib administration.

Based on *in vitro* studies, acalabrutinib is a substrate of P-glycoprotein (P-gp) and is predominantly metabolized by CYP3A enzymes.[9] Further metabolism of ACP-5862 is also mainly mediated by CYP3A. Following a single oral dose of 100 mg acalabrutinib, the half-life of ACP-5862 was 6.9 hours and the mean exposure was approximately twofold to threefold higher than that of acalabrutinib.[9] In clinical drug–drug interaction (DDI) studies with itraconazole and rifampicin, itraconazole increased acalabrutinib area under the curve (AUC) by approximately fivefold and rifampicin reduced acalabrutinib AUC to ~ 20% (about fivefold).[17] Acalabrutinib and ACP-5862 were also shown to be weak time-dependent *in vitro* inactivators of CYP3A4 and CYP2C8, respectively.[9]

A physiologically-based PK (PBPK) modeling approach was used to evaluate the DDI potential of acalabrutinib and its active metabolite, ACP-5862, after oral 100 mg twice a day (b.i.d.) administration with CYP3A inhibitors and inducers. Clinical DDI studies with a strong CYP3A inhibitor (steady-state itraconazole) or a strong inducer (steady-state rifampicin) were used to develop and verify the PBPK model. The derived PBPK model was used to evaluate the impact of potential DDIs and to define potential acalabrutinib dose adjustments. Because of the weak time-dependent inactivation of CYP3A and CYP2C8, the model was also used prospectively to predict the impact of a steady-state clinical 100 mg b.i.d. dose of acalabrutinib on exposure to the sensitive CYP3A substrate midazolam and the sensitive CYP2C8 substrate rosiglitazone.

METHODS

The acalabrutinib and ACP-5862 PBPK model was developed in two steps. The PBPK model for acalabrutinib alone was developed and verified using several different sets of clinical study data, including itraconazole and rifampicin DDI studies (**Figure 1**). After the active metabolite ACP-5862 was identified during clinical development and quantified in multiple clinical studies, the model was extended to include the metabolite. In the second stage, the acalabrutinib compound file was also updated with newly available physicochemical experimental data (logP, pKa, and blood-to-plasma partition ratio). The combined parent/metabolite model was then verified using data from two additional clinical studies (**Figure 1**). Finally, the combined PBPK model was applied to predict the potential impact of coadministration with other CYP3A inhibitors and inducers on the PK of acalabrutinib and ACP-5862 in healthy subjects. The overall modeling strategy is shown in **Figure 1**. The potential interactions between multiple oral doses of acalabrutinib and a single oral dose of midazolam or rosiglitazone were also investigated to assess the potential for acalabrutinib and ACP-5862 to perpetrate a drug interaction by inhibition of CYP3A4 or CYP2C8, respectively.

Clinical studies

ACE-HV-001 was a phase I, dose-escalation study in healthy subjects in which a single dose of 25, 50, 75, and 100 mg of acalabrutinib from cohorts 3, 4, 5, and 6, respectively, were used for model development and verification. Data from cohort 7 (N = 16), which studied a single oral dose of 50 mg acalabrutinib administered in the absence of itraconazole and on the last day of 6 consecutive days of dosing with itraconazole (200 mg b.i.d.), were used to calibrate the model for the effect of a strong CYP3A inhibitor.[17] ACE-HV-004 was a phase I, drug-interaction study in healthy subjects in which part 3 evaluated a 100 mg dose of acalabrutinib administered in the absence of rifampicin and again on the last day of 9 consecutive days of dosing with rifampicin (600 mg once a day (q.d.); N = 24),[17] which was used to verify CYP3A contribution to the overall acalabrutinib metabolism. Both studies were completed before ACP-5862 was identified, so ACP-5862 concentrations were not analyzed.

ACE-HV-005 was a phase I study to evaluate the effects of single therapeutic (100 mg) and supratherapeutic (400 mg) oral doses of acalabrutinib on the QTc interval in healthy subjects (N = 40). ACE-HV-113 was a phase I study to measure intrasubject variability in PK and determine gastric pH effects on acalabrutinib PK in healthy subjects (N = 13) after a single 100 mg dose was administered on two different occasions.[17] ACE-HV-009 was an absolute bioavailability, PK, excretion, and metabolism study of ^{14}C-acalabrutinib in healthy subjects (N = 8) in which the active metabolite was first identified and quantified.[15] When a synthetic standard and validated assay was available, ACP-5862 concentrations were measured in 18 subjects in the ACE-HV-005 study and in all subjects in the ACE-HV-113 study. Details on these clinical studies can be found in **Table 1**.

These studies were conducted in accordance with the Declaration of Helsinki and the International Conference on Harmonization/Good Clinical Practice. The final protocol and informed consent form were approved by the institutional review boards at the respective study sites. Informed consent was obtained from all volunteers before any study procedures were conducted.

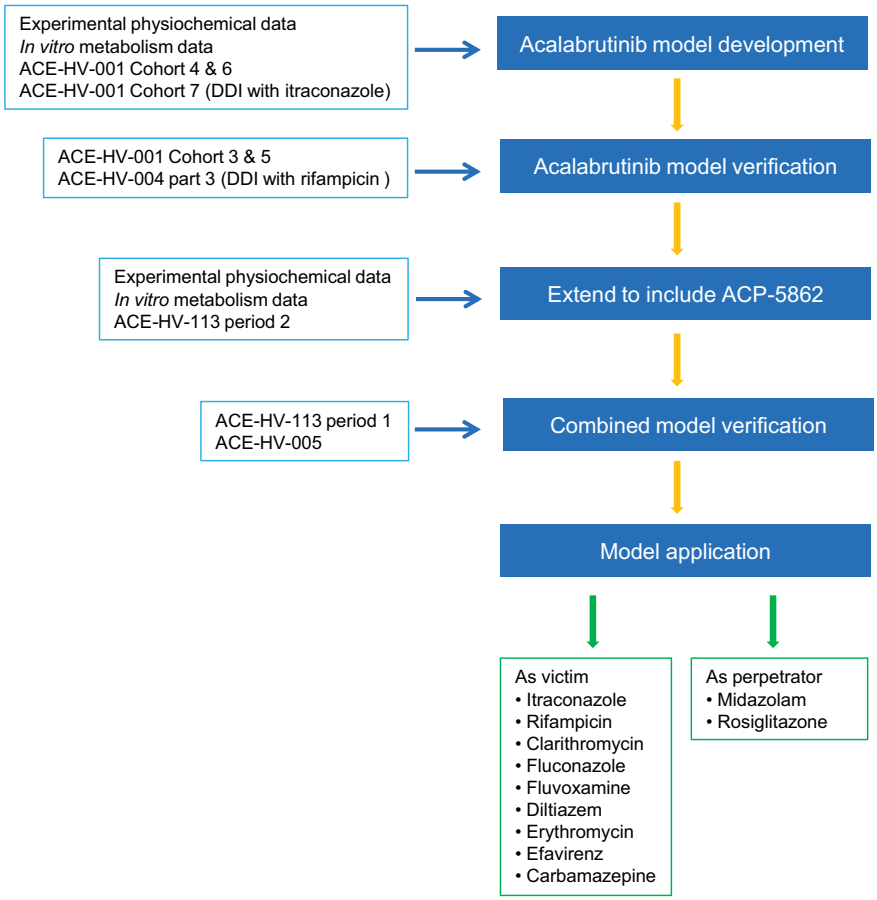

Figure 1 Flowchart for overall modeling strategy. DDI, drug–drug interaction.

Model development

Parent model. A combination of physicochemical parameters, parameters from *in vitro* absorption and metabolism studies, and concentration-time data from clinical studies (**Table 2**) were used to build a physiologically based model for acalabrutinib and ACP-5862 in Simcyp, version 14 (Certara, Sheffield, UK).[18] A minimal PBPK model with a single adjusting compartment (SAC), which considers metabolism in both the liver and intestine and lumps other tissues together, was incorporated in Simcyp for acalabrutinib. The SAC is a nonphysiological compartment that permits the adjustment of the drug concentration profiles in the systemic compartment and represents a lump of all tissues, excluding the liver and the portal vein. The concentration-time profiles of six individuals from ACE-HV-001 cohort 6 who received 100 mg acalabrutinib were used to estimate the rate of drug in and out of the SAC and the volume of the compartment using the parameter estimation module within Simcyp.

A range of human intestinal effective permeability ($P_{eff,man}$) values were investigated using the clinical results from ACE-HV-001 cohort 4 and cohort 6 (**Figure S1**), and a $P_{eff,man}$

Table 1 Summary of acalabrutinib clinical studies

Study	Dose (mg)	*N*	Age (year)	% Female	Acalabrutinib	ACP-5862
ACE-HV-001 cohort 3	25	6	30–59	83	Yes	No
ACE-HV-001 cohort 4	50	6	27–59	50	Yes	No
ACE-HV-001 cohort 5	75	12	26–56	50	Yes	No
ACE-HV-001 cohort 6	100	6	24–56	0	Yes	No
ACE-HV-001 cohort 7	50	16	19–57	19	Yes	No
ACE-HV-004 part 3	100	24	18–58	33	Yes	No
ACE-HV-113	100	12	18–58	33	Yes	Yes
ACE-HV-005	100, 400	18	19–63	40	Yes	Yes
ACE-HV-009	100	14	18–65	36	Yes	Yes, semiquantitive

The last two columns indicate if acalabrutinib and/or ACP-5862 were measured in the specific study.

Table 2 Input parameters used to simulate the kinetics of acalabrutinib and ACP-5862

	Acalabrutinib		ACP-5862	
Parameter	**Value**	**Source**	**Value**	**Source**
Molecule weight	465.5	Experimental data	481.5	Experimental data
logP	2.03	Experimental data	2.72	Experimental data
Compound type	Diprotic base	Experimental data	Diprotic base	Experimental data
pKa	3.54, 5.77	Experimental data	3.41, 4.49	Experimental data
B/P ratio	0.787	Experimental data	0.65	Experimental data
$f_{u,plasma}$	0.026	Experimental data	0.013	Experimental data
f_a	0.98	Predicted	—	—
k_a ($hour^{-1}$)	1.65	Predicted	—	—
Lag time (hour)	0.25	Optimized	—	—
Q_{gut} (L/hour)	12.33	Predicted	—	—
$f_{u,gut}$	0.026	Equal to fup	—	—
$P_{eff,man}$ ($\times 10^{-4}$ cm/second)	4	Optimized based on clinical data	—	—
V_{ss} (L/kg)	0.21	Predicted (Rodgers and Rowland method)	0.36	Predicted (Rodgers and Rowland method)
V_{sac} (L/kg)	0.028	Parameter estimation	0.1	Parameter estimation
k_{in} (1/hour)	1.06	—	0.32	—
k_{out} (1/hour)	0.45	—	0.01	—
fmCYP3A4	0.82	Optimized based on clinical data	—	—
CYP3A4 CL_{int} (μL/minutes/pmol)	9.63	Retrograde model, total CYP3A4 clearance	—	—
CYP3A4 V_{max} (pmol/minutes/pmol)	4.13	Experimental data, convert to ACP-5862	—	—
CYP3A4 K_m (μM)	2.78	Experimental data, convert to ACP-5862	—	—
CYP3A4 CL_{int} (μL/minutes/pmol)	8.14	The rest to other metabolites	—	—
Additional HLM (μL/minutes/mg)	289.5	Retrograde model	—	—
Clint *in vitro* HLM (μL/minutes/mg) CYP3A4	—	—	23.6	Experimental data
CLR (L/hour)	1.33	Clinical data	0.3	Clinical data
CYP2C8 Ki (μM)	20.6	Experimental data	—	—
CYP2C9 Ki (μM)	11.3	Experimental data	3.35	Experimental data
CYP2C19 Ki (μM)		Experimental data	8.5	Experimental data
CYP3A4 Ki (μM)	23.9	Experimental data	—	—
CYP3A4 KI (μM)	10.1	Experimental data	—	—
CYP3A4 kinact (1/hour)	1.11	Experimental data	—	—
CYP2C8 kinact (1/hour)	—	—	0.72	Experimental data
CYP2C8 KI (μM)	—	—	4	Experimental data

B/P, blood-to-plasma ratio; CLint, intrinsic clearance; $f_{u,gut}$, fraction unbound in enterocyte; $f_{u,plasma}$, unbound fraction in plasma; fa, fraction of absorption; fa, fraction of absorption; fm, fraction of metabolism; HLM, human liver microsome; ka, rate of absorption; Ki, inhibitory constant for reversible inhibition; KI, inhibitory constant for time-dependent inhibition; kin, kout, first order rate constants inand out Vsac; Kinact, rate of enzyme inactivation; Km, Michaelis-Menten constant; Peff,man, human intestinal effective permeability; pKa, acid dissociation constant (logarithmic scale); Qgut, nominal flow through the gut; Vmax, maximum rate of metabolism formation; Vsac, volume of single adjusting compartment; Vss, volume of distribution at steady state.

value of 4.0×10^{-4} cm/second was most consistent with the observed acalabrutinib peak plasma concentration (C_{max}) values and was therefore applied in the model. The volume of distribution at steady state was predicted using logP, pKa, and blood-to-plasma partition ratio values by the Rodgers and Rowland[19] method. Fraction unbound in enterocyte was assumed to be the same as unbound fraction in plasma (**Table 2**).

In vitro incubation of 20 μM ^{14}C-acalabrutinib (for qualitative metabolite profiling) with human hepatocytes (two male donors, CellzDirect-Invitrogen, Austin, TX) indicated relative contributions of glutathione and CYP-mediated metabolic pathways of 21% and 79%, respectively, and the CYP3A enzyme was the main enzyme (~ 90%) involved in the formation of CYP metabolites (data on file). Eventually, the percentage of acalabrutinib metabolized by CYP3A4 was assigned as 0.82 based on itraconazole interaction study ACE-HV-001, cohort 7. The renal clearance of 1.33 L/hour for acalabrutinib observed in clinical study ACE-HV-009[15] was applied directly. The intrinsic metabolic clearance of acalabrutinib was estimated from the *in vivo* total clearance of 169 L/hour (ACE-HV-001) with the retrograde method. The total intrinsic metabolic clearance was then separated into CYP3A4 and undefined components based on the percentage of acalabrutinib metabolized by CYP3A4. The intrinsic clearance value of 9.63 μL/minutes/pmol was assigned for CYP3A4 with

289.5 μL/minutes/mg for additional human liver microsome clearance for the elimination of acalabrutinib (**Table 2**).

In vitro studies using MDCKII-MDR1 cells (Netherlands Cancer Institute, Amsterdam, The Netherlands) indicated that acalabrutinib is a substrate of P-gp with efflux ratio (42 at 1 μM; data on file). In the absence of detailed information on the specificity and affinity of acalabrutinib for transport, it was not possible to include the active transport process in the model. However, the sensitivity of the final parent model to the impact of intestinal efflux was investigated using the advanced dissolution, absorption and metabolism model within Simcyp in conjunction with a range of *in vitro* intestinal P-gp maximum rate of transporter mediated efflux and Michaelis-Menten constant (K_m) values.

Combined parent and metabolite model. The combined parent metabolite model was developed as an extension of the parent-alone model (**Table 2**). The logP, pKa, and blood-to-plasma partition ratio of acalabrutinib in the parent-alone model were updated with experimental values. The volume of distribution at steady state of 0.36 L/kg for ACP-5862 was predicted using the Rodgers and Rowland[19] method. A SAC was also applied for the metabolite, and the concentration-time profile from the ACE-HV-113 period 2 oral dose (100 mg acalabrutinib) were used to optimize the volume of SAC and the rate of drug in and out of the SAC for ACP-5862.

The metabolism of acalabrutinib to ACP-5862 was characterized in recombinant CYP enzymes, and CYP3A4 was identified as the sole enzyme responsible for the conversion of acalabrutinib to ACP-5862. The reported maximum rate of metabolism formation (V_{max}) of 4.13 pmol/minutes/pmol and K_m of 2.78 μM in CYP3A4 were incorporated in the model to describe the conversion of acalabrutinib to ACP-5862. Therefore, the elimination of acalabrutinib via CYP3A4 (9.63 μL/minutes/pmol) was further divided into two clearance pathways: one to the active metabolite ACP-5862 (V_{max} of 4.13 pmol/minutes/pmol and K_m of 2.78 μM) and the other to the rest of the metabolites (8.14 μL/minutes/pmol). The *in vitro* studies also demonstrated that the CYP3A enzyme was responsible for the further metabolism of ACP-5862, and a clearance value of 23.6 μL/minutes/mg protein in human liver microsomes was assigned to CYP3A4 for the elimination of ACP-5862. A renal clearance of 0.3 L/hour for ACP-5862 reported in ACE-HV-009[17] was applied in the model. Such assignment suggested that the ACP-5862–related metabolites contributed about 12% of total acalabrutinib elimination, which is in close agreement with the 10% of total dose observed in human mass balance study.[15]

The competitive and time-dependent inhibition parameters against the CYP2C8, CYP2C9, CYP2C19, and CYP3A enzymes obtained from *in vitro* studies were applied for both acalabrutinib and ACP-5862 (**Table 2**). Acalabrutinib did not cause significant induction of the metabolism of the marker substrates of CYP1A2, CYP2B6, or CYP3A4 at any concentration evaluated.

Model verification

The parent-alone model was verified with the clinical study ACE-HV-001 cohort 3 and cohort 5, in which a single dose of 25 and 75 mg of acalabrutinib was given, as well as ACE-HV-004 part 3, in which acalabrutinib in the absence and presence of multiple doses of rifampicin was evaluated. The combined parent and metabolite model was verified again with the DDI studies with itraconazole and rifampicin. The model was also verified with studies ACE-HV-005 and ACE-HV-113 period 1, in which both acalabrutinib and its active metabolite were measured (**Table S1**). Default compound files for the CYP3A4 substrate midazolam and the CYP2C8 substrate rosiglitazone were applied directly. Simulations of the DDIs between itraconazole and midazolam or gemfibrozil and rosiglitazone were conducted to verify these two compound files.

Default Simcyp parameter values for creating a virtual North European Caucasian or virtual Healthy Volunteer population (population, physiological parameters including liver volume and blood flows, enzyme abundances) were applied in the current analysis.[20] All simulations were run with virtual subjects matched as closely as possible with respect to age and sex to those in the corresponding actual clinical studies and according to the same study design as summarized in **Table 1**. The detailed simulation condition for each study can be found in **Table S1**.

Model application

Various clinical DDI scenarios were simulated using the final model of acalabrutinib and ACP-5862 to evaluate the likely impact of the coadministration of multiple doses of CYP3A4 inhibitors and inducers on the kinetics (C_{max} and AUC) of both acalabrutinib and ACP-5862 in healthy subjects. The AUC ratios of acalabrutinib and ACP-5862 in the absence and presence of a CYP3A inhibitor or inducer were calculated. The total active component (acalabrutinib plus ACP-5862) in the absence and presence of a CYP3A inhibitor or inducer were also determined as sum of the AUC of acalabrutinib and ACP-5862. In addition, ACP-5862 exposure was further adjusted for its potency for BTK inactivation relative to the parent acalabrutinib.

Because acalabrutinib and ACP-5862 exhibited as time-dependent inhibitors of CYP3A4 and CYP2C8, respectively, from *in vitro* studies (**Table 2**), the potential interactions between multiple 100 mg b.i.d. oral doses of acalabrutinib and a single oral dose of midazolam or rosiglitazone were investigated to assess the potential for acalabrutinib and ACP-5862 to inhibit CYP3A4 or CYP2C8. Compound files were used as provided by the Simcyp software for all CYP3A inhibitors (itraconazole, clarithromycin, fluconazole, fluvoxamine, diltiazem, erythromycin), inducers (rifampicin, efavirenz, carbamazepine) and substrate (midazolam) and CYP2C8 substrate (rosiglitazone). The detailed simulation condition for each interaction study design is provided in **Table S1**.

RESULTS

The initial simulations of the PK of acalabrutinib alone (ACE-HV-001 cohorts 4 and 6) and in the presence of itraconazole (ACE-HV-001 cohort 7) were used to optimize the parameter inputs for the parent-alone model (**Figure 1**). Simulated profiles for the acalabrutinib and itraconazole interactions were then compared with observed data (**Figure S2**). The model was further verified with two additional clinical studies

(ACE-HV-001 cohorts 3 and 5) and the rifampicin interaction (ACE-HV-004 part 3; **Figure S2**). The predicted AUC values and AUC ratios were in close agreement to the observed values, indicating that the model adequately captures the kinetics of acalabrutinib. A sensitivity analysis was conducted using the parent-alone model to investigate the impact of the intestinal efflux on the C_{max} and AUC (**Figure S3**). There was a slight change in the acalabrutinib exposure only when an extreme high maximum rate of transporter-mediated efflux and low K_m were applied, suggesting that the efflux process is unlikely to be of clinical significance; hence, this component was not included in further modeling.

The parent-alone model was then extended to capture the active metabolite of acalabrutinib after ACP-5862 was identified in the human mass balance study (ACE-HV-009), and the metabolite PK from study ACE-HV-113 period 2 was applied to optimize the parameter inputs for ACP-5862. The combined model was verified by comparing the predicted kinetic profiles and exposure for both acalabrutinib and ACP-5862 after a 100 mg single dose of acalabrutinib with observed values (**Table S2**). The combined model predicted the AUC values of acalabrutinib and ACP-5862 and was in close agreement with the reported values for both studies (**Table S2**). Simulated concentration profiles for acalabrutinib and ACP-5862 in comparison with the observed data are presented in **Figure 2**. The model slightly underestimated the acalabrutinib exposure, but not the metabolite exposure, after a 400 mg single dose, and this was potentially because of a greater-than-proportional increase in AUC between the 100 and 400 mg doses in study ACE-HV-005 (**Table S2**).

The combined model was reverified by comparing the predicted PK changes in acalabrutinib with the coadministration of itraconazole 200 mg b.i.d. or rifampin 600 mg q.d. with observed changes. The predicted and observed changes in the AUC and C_{max} ratio with concomitant itraconazole were 4.80-fold and 5.21-fold (AUC) and 3.23-fold and 3.90-fold (C_{max}), respectively (**Table S3, Figure 3**). With the coadministration of rifampin, the predicted and observed decreases in the AUC ratio were 0.21-fold and 0.23-fold, respectively, and the predicted and observed decreases in the C_{max} ratio were 0.24-fold and 0.32-fold (**Table S3**). The simulated concentration profiles for the acalabrutinib interaction with itraconazole and rifampin relative to the observed data are presented in **Figure 3**. The reasonable predictions of acalabrutinib and ACP-5862 exposure (**Table S2**) and the acalabrutinib AUC and C_{max} ratios with coadministered itraconazole and rifampin (**Table S3**) also demonstrate that the assigned parameters were appropriate to predict changes in the acalabrutinib and ACP-5862 plasma concentration-time profiles during potential drug interactions.

After the verification of the acalabrutinib and ACP-5862 PBPK model, it was applied to predict untested clinical outcomes for DDIs with other CYP3A inhibitors or inducers. The moderate CYP3A inhibitors fluconazole, diltiazem, and erythromycin were predicted to increase steady-state acalabrutinib AUC by 2.44-fold, 2.28-fold, and 2.76-fold, respectively. The weak CYP3A inhibitor fluvoxamine was predicted to increase steady-state acalabrutinib AUC by 37%. The model also predicted that the steady-state acalabrutinib AUC would decrease by 61% in the presence of CYP3A inducer efavirenz or carbamazepine (**Table S4**).

When acalabrutinib was coadministered at 100 mg b.i.d. at the end of a multiple-dose itraconazole regimen (200 mg b.i.d. for 6 days), the predicted acalabrutinib geometric mean AUC was about 4.59-fold higher relative to acalabrutinib given alone. However, the ACP-5862 AUC was significantly reduced in the presence of itraconazole, 0.15-fold when compared with acalabrutinib given alone (**Table S4**). Therefore, the total active component (acalabrutinib plus ACP-5862) in the presence of itraconazole was within 6% of the total active component when acalabrutinib was given in the absence of itraconazole, indicating that even with a fivefold increase in parent AUC, there was little net change in the total AUC of the two active components (parent and metabolite) in the presence of a strong CYP3A4 inhibitor. Simulations showed similar outcomes when acalabrutinib 100 mg b.i.d. was coadministered with moderate or weak CYP3A4 inhibitors, such as diltiazem and fluconazole (**Table S4**). Similarly, the ratios of total exposure by considering the relative BTK potency between acalabrutinib and ACP-5862 in the absence and presence of CYP inhibitors/inducers has also been presented in **Table S4**, which are similar as ratios of total exposure without considering the relative BTK potency. The simulated DDIs are summarized as a forest plot in **Figure 4**.

When 100 mg b.i.d. acalabrutinib was coadministered with a multiple-dose regimen of the strong CYP3A inducer rifampin (600 mg q.d. for 9 days), even though parent-drug AUC was decreased by fivefold to 17% of control exposure, the predicted geometric mean total AUC of the two active components (acalabrutinib plus ACP-5862) decreased by only twofold (46% of acalabrutinib alone). At an acalabrutinib dose of 200 mg b.i.d., the simulation indicated exposure to acalabrutinib plus metabolite would be 92% of the exposure to acalabrutinib 100 mg b.i.d. without rifampin (**Table S4 and Figure 4**). Similarly, in the presence of the moderate CYP3A inducer efavirenz, the combined AUC of acalabrutinib and ACP-5862 decreased by 1.3-fold (75% of acalabrutinib alone).

The combined model was also applied to predict the impact of multiple 100 mg b.i.d. doses of acalabrutinib as a perpetrator on the sensitive substrates of CYP3A and CYP2C8. The predicted geometric mean midazolam AUC and C_{max} ratios were 1.03 and 1.02, respectively, in the presence and absence of acalabrutinib coadministration. Similarly, the predicted geometric mean rosiglitazone AUC and C_{max} ratio was 1.02 and 1.00, respectively, indicating that acalabrutinib has little effect on CYP3A or CYP2C8 enzyme levels.

DISCUSSION

PBPK modeling has been widely used in drug development to support development decisions, pediatric dose selection, and regulatory submissions and labeling.[21–25] In the current analysis, a PBPK model of acalabrutinib and its metabolite ACP-5862 was developed by integrating physiochemical properties, *in vitro* metabolism data, and clinical PK results and was subsequently verified using available

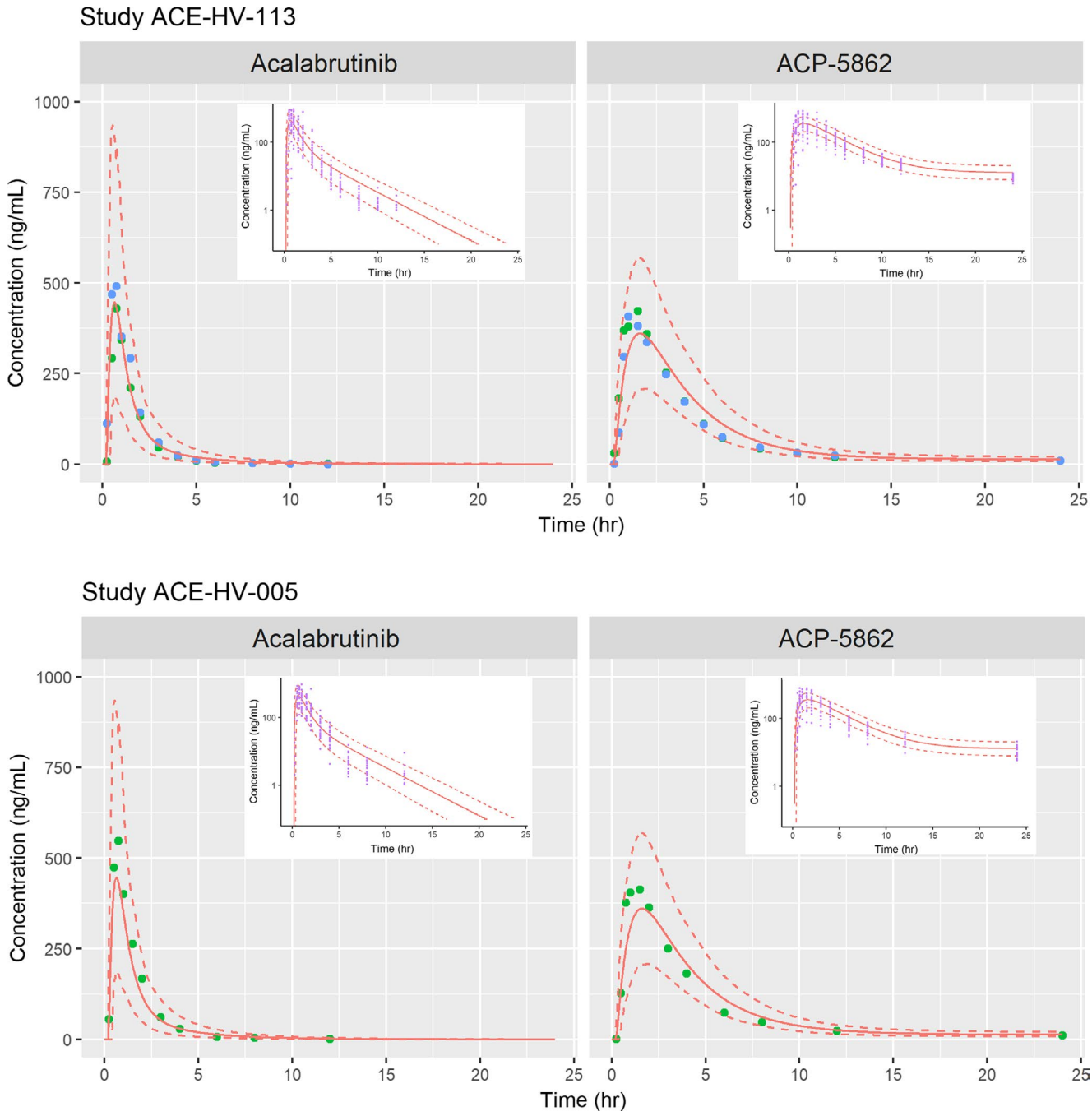

Figure 2 Plasma concentrations of acalabrutinib and ACP-5862 after single oral dosing of 100 mg acalabrutinib in healthy volunteers for study ACE-HV-113 and ACE-HV-005. Simulated values are displayed as lines, including means (solid lines) and 5% and 95% percentiles (dashed lines). Observed data from clinical studies are displayed as solid dots. Inserts show semilog plots of individual observations. hr, hour.

DDI clinical data and then applied to prospective predictions of acalabrutinib-drug combinations for which no clinical data were available.

The PK of acalabrutinib was linear in the therapeutic range of 75–250 mg, although a slightly higher than proportional exposure was observed at the 400 mg dose. *In vitro* studies indicated that acalabrutinib is a substrate of P-gp with an efflux ratio around half that of the established P-gp substrate digoxin, and acalabrutinib is not a P-gp inhibitor. Sensitivity analysis indicated a slight change in acalabrutinib exposure only when extreme high affinity was applied (**Figure S3**). In addition, the unchanged acalabrutinib accounted for only 1.2% of the excreted dose in the human mass-balance study,[15] suggesting a negligible P-gp contribution to the acalabrutinib PK. Considering the linear PK for acalabrutinib at a therapeutic dose of 100 mg, the

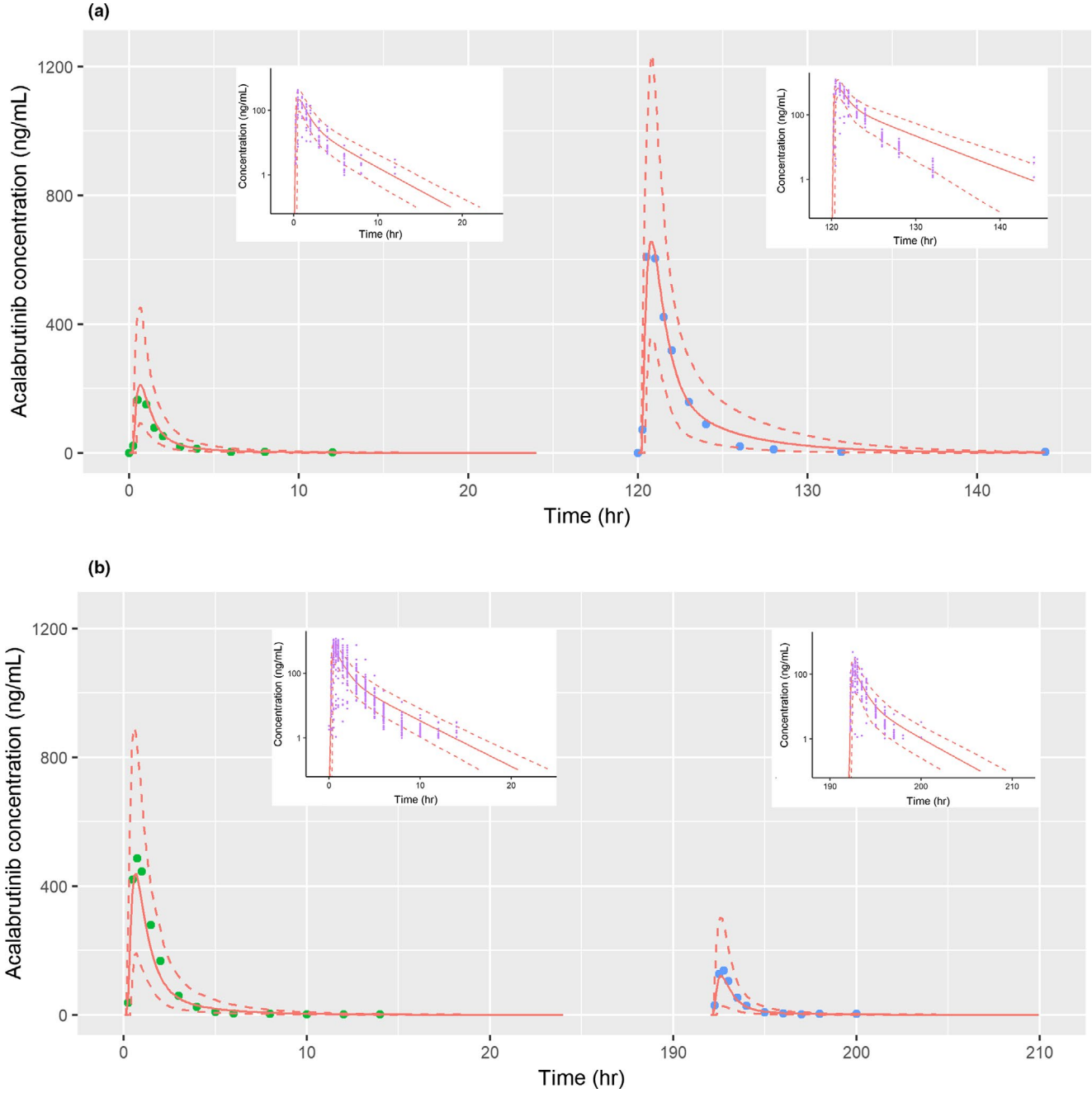

Figure 3 Simulated plasma drug concentration-time profiles for acalabrutinib alone and in the presence of the (**a**) CYP3A inhibitor itraconazole 200 mg twice a day or (**b**) CYP3A inducer rifampin 600 mg once a day. A single oral dose of 50 mg acalabrutinib administered in the absence of itraconazole and on the last day of 6 days of dosing with itraconazole (200 mg twice a day) is shown in **a**, and a single oral dose of 100 mg acalabrutinib administered in the absence of rifampicin and on the last day of 9 days of dosing with rifampicin (600 mg once a day) is shown in **b**. Simulated values are displayed as lines, including means (solid lines) and 5% and 95% percentiles (dashed lines). Observed data from clinical studies are displayed as solid dots. Green and blue dots indicate the acalabrutinib alone or in the presence of interaction, respectively. Inserts show semilog plots of individual observations. hr, hour.

efflux process is unlikely to be of clinical significance for acalabrutinib absorption. The *in vitro* study indicated that acalabrutinib was a weak inhibitor of CYP3A, CYP2C8, and CYP2C9 and a time-dependent inhibitor of CYP3A with a K_I value (the concentration at half of the maximal inactivation rate) of 10.1 μM. However, the competitive and time-dependent inhibition has minimal clinical impact, and even though acalabrutinib is mainly metabolized by CYP3A, time-dependent accumulation of acalabrutinib was not observed. In addition, the model also predicted that steady-state exposure to acalabrutinib and ACP-5862 is almost the same, with or without consideration of the time-dependent inhibition.

The elimination of acalabrutinib was estimated using *in vivo* oral clearance observed in a phase I clinical study, and

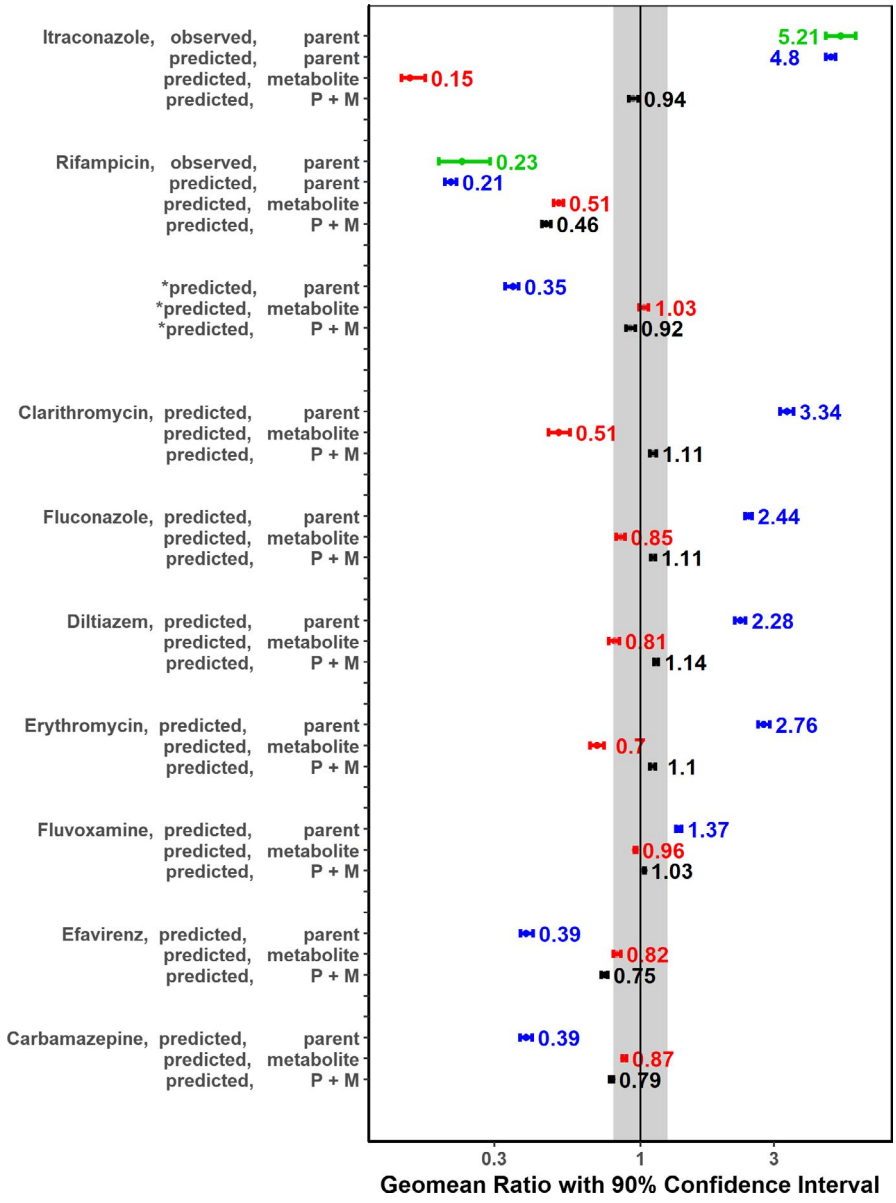

Figure 4 Summary of all drug–drug interaction predictions. Ratio of geometric means in drug–drug interaction simulations. All simulations were performed for 100 mg twice a day of acalabrutinib in the absence and presence of different CYP3A inhibitor/inducer. *, shows the ratio of 200 acalabrutinib plus rifampicin twice a day vs. 100 acalabrutinib alone twice a day. The dots and numbers nearby are the geometric mean of ratios in each scenario, and the horizontal segments are the 90% confidence intervals of the geometric mean. Green indicates the observed values in itraconazole and rifampicin clinical drug–drug interaction studies (ACE-HV-001 cohort 7 and ACE-HV-004 part 3), which was a single dose of acalabrutinib with/without itraconazole or rifampicin. Blue indicates the values calculated for parent only. Red indicates the values calculated for metabolite only. The values in black are the ratios calculated considering the total component of parent and metabolite (P+M). Gray area is the 80–125% criteria for bioequivalence.

the fraction metabolized by CYP3A4 was determined using the itraconazole interaction study. Total CYP3A metabolism was further divided into two portions: one to its active metabolite ACP-5862, which was determined by *in vitro* study using recombinant CYP3A4 enzyme, and another to the rest of the metabolism of acalabrutinib. The current model also applied CYP3A4 as the only enzyme involved in the further metabolism of ACP-5862 based on *in vitro* experiments. Sensitivity analysis of a CYP3A4 fraction for the elimination of ACP-5862 was conducted. With a lower CYP3A4 fraction, the AUC of ACP-5862 did increase in the presence of multiple doses of rifampicin, but the overall increase was not significant (data not shown). Application of these two sets of *in vitro* parameters to the formation and elimination of ACP-5862 reasonably capture the ACP-5862 PK profile in both 100 mg and 400 mg dose groups, indicating that this *in vitro* to *in vivo* extrapolation works well for ACP-5862.

One of the limitations of the available data is the lack of confirmation of the metabolite exposure in CYP3A inhibition and induction studies that are needed to confirm the

predictions for the metabolite exposures are appropriate. However, the PBPK model predicted PK of both parent and metabolite under no DDI conditions at the clinically relevant dose of 100 mg (**Table S3**). The final PBPK model also adequately predicted an acalabrutinib exposure increase and decrease with a strong CYP3A inhibitor and inducer, respectively (**Table S4**). Therefore, the model was appropriate to use with confidence to predict the magnitude of DDIs for acalabrutinib and its metabolite as victims of a CYP3A-mediated DDI. PBPK simulations with acalabrutinib and moderate CYP3A inhibitors (erythromycin, fluconazole, diltiazem) showed that coadministration increased acalabrutinib C_{max}, and AUC increased by twofold to almost threefold (**Table S5**), resulting in a recommendation for a dose reduction to 100 mg q.d. when acalabrutinib is coadministered with moderate CYP3A inhibitors, per the US package insert.[9] However, the total active component (acalabrutinib plus ACP-5862) exposure had negligible change in the presence of moderate CYP3A inhibitors because of the ACP-5862 exposure reduction in the presence of these inhibitors. Currently, clinical information is being compiled to confirm such predictions, which may provide more precise dosing recommendations in the presence of strong or moderate CYP3A inhibitors. Based on *in vitro* data and PBPK modeling, no interaction with sensitive CYP2C8 or CYP3A substrates is expected at clinically relevant concentrations of acalabrutinib.[9] The model also predicted that exposures of total active component (acalabrutinib plus metabolite) at 200 mg b.i.d. in the presence of rifampicin would be similar to those at 100 mg b.i.d. without the rifampicin interaction. Therefore, the US package insert suggests to avoid concomitant use of strong CYP3A inducers, and if these inducers cannot be avoided, increase the acalabrutinib dose to 200 mg twice daily.[9]

With support of clinical data, only a limited number of drugs, including gefitinib,[26] erlotinib,[27] and osimertinib,[28] have recommendations to increase dose in the presence of strong CYP inducers. In this study, acalabrutinib provided a case for a dose increase based on the PBPK model. The model also adequately predicted a 4.8-fold acalabrutinib AUC increase in the presence of itraconazole, similar to the observed 5.2-fold change (**Table S4**). Considering the significant ACP-5862 exposure reduction in the presence of itraconazole, the predicted total active component (acalabrutinib plus ACP-5862) exposure was similar in the absence or presence of a strong CYP3A inhibitor. Similarly, a clinical study showed that the strong CYP3A inhibitor clarithromycin increased abemaciclib exposure by 3.4-fold, but only increased the total active species (abemaciclib plus its three active metabolites) by 2.2-fold,[29] and the US label recommended an abemaciclib dose reduction in the presence of strong CYP3A inhibitors (except ketoconazole) to 100 mg twice daily from 200 or 150 mg twice daily.[30] From an efficacy point of view, dose adjustment may not be necessary when acalabrutinib is coadministered with strong CYP3A inhibitors. However, there are no long-term safety data available for acalabrutinib at doses higher than 400 mg, so the potential impact of the fivefold increase in acalabrutinib exposure on safety remains unclear. As such, the current US label recommends avoiding coadministration with strong CYP3A inhibitors.[9] This recommendation for acalabrutinib to be used with strong CYP3A inhibitors is similar to that of ibrutinib, even though ibrutinib has much larger interactions with CYP3A inhibitors and inducers (29-fold increase with the strong CYP3A inhibitor ketoconazole and a 20-fold decrease with the strong inducer rifampicin).[31]

In conclusion, the PBPK model adequately captured the PK profiles of acalabrutinib and its active metabolite ACP-5862 as well as parent, metabolite, and total parent and metabolite (total active component) exposure in drug interactions with CYP3A inhibitors and inducers. The model indicated that there was little change in exposure to total active component in the presence of strong or moderate CYP3A inhibitors and only a 50% decrease in exposure to total active components in the presence of a strong CYP3A inducer. The PBPK model guided package insert dose change recommendations for CYP3A inhibitors and inducers and also showed that acalabrutinib is unlikely to perpetrate a drug interaction on sensitive CYP2C8 or CYP3A substrates.

Supporting Information. Supplementary information accompanies this paper on the *CPT: Pharmacometrics & Systems Pharmacology* website (www.psp-journal.com).

Supplementary Figures and Tables

Table S1. Trial design for each simulation.

Table S2. The predicted and observed geometric mean AUC and C_{max} with coefficient of variation (%CV) of acalabrutinib and ACP-5862.

Table S3. The predicted and observed geometric mean acalabrutinib AUC and C_{max} and geometric mean ratio in the absence and presence of itraconazole and rifampin.

Table S4. The predicted geometric mean ratio of acalabrutinib, ACP-5862, and total active component (acalabrutinib plus ACP-5862) in the absence and presence of different CYP3A inhibitors and inducers.

Figure S1. Evaluation of the impact of $P_{eff,man}$ on the C_{max} of acalabrutinib.

Figure S2. Mean simulated and observed plasma concentrations of acalabrutinib using parent-alone PBPK model.

Figure S3. A sensitivity analysis to determine the impact of *in vitro* intestinal P-gp J_{max} and K_m values on acalabrutinib (a) f_a, (b) C_{max}, and (c) AUC after a single oral dose of 100 mg acalabrutinib.

Acknowledgments. The authors thank Zoe Barter and Karen Rowland Yeo from Certara for initial model development. The authors also thank Jingtao Lu and Eric Masson for model development and valuable discussions. The authors thank the patients and volunteers for their participation in the clinical studies.

Funding. This study was funded by Acerta Pharma (a member of the AstraZeneca group, South San Francisco, California) and AstraZeneca (Boston, Massachusetts).

Conflict of Interest. D.Z., G.M., K.V., and N.A. are employees of and shareholders in AstraZeneca. Y.X. and J.W. are employees of Acerta Pharma, and T.P. and J.G.S. are former employees of Acerta Pharma and shareholders in AstraZeneca.

Author Contributions. All authors wrote the manuscript. D.Z., J.G.S., T.P., and Y.X. designed the research. D.Z. and G.M. performed the research. T.P. and Y.X. analyzed the data.

1. Küppers, R. Mechanisms of B-cell lymphoma pathogenesis. *Nat. Rev. Cancer* **5**, 251–262 (2005).
2. Shaffer, A.L., Rosenwald, A. & Staudt, L.M. Lymphoid malignancies: the dark side of B-cell differentiation. *Nat. Rev. Immunol.* **2**, 920–932 (2002).
3. Gayko, U. *et al.* Development of the Bruton's tyrosine kinase inhibitor ibrutinib for B cell malignancies. *Ann. N.Y. Acad. Sci.* **1358**, 82–94 (2015).
4. Hendriks, R.W., Yuvaraj, S. & Kil, L.P. Targeting Bruton's tyrosine kinase in B cell malignancies. *Nat. Rev. Cancer* **14**, 219–232 (2014).
5. Byrd, J.C. *et al.* Acalabrutinib (ACP-196) in relapsed chronic lymphocytic leukemia. *N. Engl. J. Med.* **374**, 323–332 (2016).
6. Buggy, J.J. & Elias, L. Bruton tyrosine kinase (BTK) and its role in B-cell malignancy. *Int. Rev. Immunol.* **31**, 119–132 (2012).
7. Covey, T. *et al.* ACP-196: a novel covalent Bruton's tyrosine kinase (Btk) inhibitor with improved selectivity and *in vivo* target coverage in chronic lymphocytic leukemia (CLL) patients. *Can. Res.* **75**, 2596 (2015).
8. Barf, T. *et al.* Acalabrutinib (ACP-196): a covalent Bruton tyrosine kinase (BTK) inhibitor with a differentiated selectivity and *in vivo* potency profile. *J. Pharmacol. Exp. Ther.* **363**, 240–252 (2017).
9. US Food and Drug Administration. CALQUENCE (acalabrutinib) capsules: highlights of prescribing information <https://www.accessdata.fda.gov/drugsatfda_docs/label/2017/210259s000lbl.pdf>.
10. Farrukh, T.A. & Wojciech, J. Use of acalabrutinib in patients with mantle cell lymphoma. *Exp. Rev. Hematol.* **11**, 495–502 (2018).
11. Honigberg, L.A. *et al.* The Bruton tyrosine kinase inhibitor PCI-32765 blocks B-cell activation and is efficacious in models of autoimmune disease and B-cell malignancy. *Proc. Natl. Acad. Sci. USA* **107**, 13075–13080 (2010).
12. Golay, J., Ubiali, G. & Introna, M. The specific Bruton tyrosine kinase inhibitor acalabrutinib (ACP-196) shows favorable *in vitro* activity against chronic lymphocytic leukemia B cells with CD20 antibodies. *Haematologica* **102**, e400–e403 (2017).
13. Patel, V. *et al.* Comparison of acalabrutinib, a selective Bruton tyrosine kinase inhibitor, with ibrutinib in chronic lymphocytic leukemia cells. *Clin. Cancer Res.* **23**, 3734–3743 (2017).
14. Wang, M. *et al.* Acalabrutinib in relapsed or refractory mantle cell lymphoma (ACE-LY-004): a single-arm, multicentre, phase 2 trial. *Lancet* **391**, 659–667 (2018).
15. Podoll, T. *et al.* Bioavailability, biotransformation, and excretion of the covalent BTK inhibitor acalabrutinib in rats, dogs, and humans. *Drug Metab. Dispos.* **47**, 145–154 (2019).
16. Edlund, H., Lee, S.K., Andrew, M.A., Slatter, J.G., Aksenov, S. & Al-Huniti, N. Population pharmacokinetics of the BTK inhibitor acalabrutinib and its active metabolite in healthy volunteers and patients with B-cell malignancies. *Clin. Pharmacokinet.* https://doi.org/10.1007/s40262-018-0725-7. [e-pub ahead of print].
17. Izumi, R. *et al.* CYP3A-mediated drug interaction profile of bruton tyrosine kinase inhibitor, Acalabrutinib. *Blood* **130**, 4996 (2017).
18. Jamei, M., Marciniak, S., Feng, K., Barnett, A., Tucker, G. & Rostami-Hodjegan, A. The Simcyp population-based ADME simulator. *Expert Opin. Drug Metab. Toxicol.* **5**, 211–223 (2009).
19. Rodgers, T. & Rowland, M. Mechanistic approaches to volume of distribution predictions: understanding the processes. *Pharm. Res.* **24**, 918–933 (2007).
20. Howgate, E.M., Rowland Yeo, K., Proctor, N.J., Tucker, G.T. & Rostami-Hodjegan, A. Prediction of *in vivo* drug clearance from *in vitro* data. I: impact of inter-individual variability. *Xenobiotica* **36**, 473–497 (2006).
21. Johnson, T.N., Zhou, D. & Bui, K.H. Development of physiologically based pharmacokinetic model to evaluate the relative systemic exposure to quetiapine after administration of IR and XR formulations to adults, children and adolescents. *Biopharm. Drug Dispos.* **35**, 341–352 (2014).
22. Zhou, D., Bui, K., Sostek, M. & Al-Huniti, N. Simulation and prediction of the drug-drug interaction potential of naloxegol by physiologically based pharmacokinetic modeling. *CPT Pharmacometrics Syst. Pharmacol.* **5**, 250–257 (2016).
23. Chen, Y., Zhou, D., Tang, W., Zhou, W., Al-Huniti, N. & Masson, E. Physiologically based pharmacokinetic modeling to evaluate the systemic exposure of gefitinib in CYP2D6 ultrarapid metabolizers and extensive metabolizers. *J. Clin. Pharmacol.* **58**, 485–493 (2018).
24. Pilla Reddy, V., Bui, K., Scarfe, G., Zhou, D. & Learoyd, M. Physiologically based pharmacokinetic modeling for olaparib dosing recommendations: bridging formulations, drug interactions, and patient populations. *Clin. Pharmacol. Ther.* **105**, 229–241 (2019).
25. Al-Huniti, N. *et al.* Pharmacometric modeling of naloxegol efficacy and safety: impact on dose and label. *Clin. Pharmacol. Ther.* **102**, 741–744 (2017).
26. US Food and Drug Administration. IRESSA (gefitinib) tablets: highlights of prescribing information <https://www.accessdata.fda.gov/drugsatfda_docs/label/2015/206995s000lbl.pdf>.
27. US Food and Drug Administration. TARCEVA (erlotinib) tablets: highlights of prescribing information <https://www.accessdata.fda.gov/drugsatfda_docs/label/2010/021743s14s16lbl.pdf>.
28. US Food and Drug Administration. TAGRISSO (osimertinib) tablets: highlights of prescribing information <https://www.accessdata.fda.gov/drugsatfda_docs/label/2015/208065s000lbl.pdf>.
29. Kulanthaivel, P. *et al.* Pharmacokinetic drug interactions between abemaciclib and CYP3A inducers and inhibitors. Proceedings of the 107th Annual Meeting of the American Association for Cancer Research, New Orleans, LA, April 16–20, 2016. Abstract CT153.
30. US Food and Drug Administration. VERZENIO (abemaciclib) tablets: highlights of prescribing information <https://www.accessdata.fda.gov/drugsatfda_docs/label/2017/208716s000lbl.pdf>.
31. US Food and Drug Administration. IMBRUVICA (ibrutinib) capsules: highlights of prescribing information <https://www.accessdata.fda.gov/drugsatfda_docs/label/2015/205552s002lbl.pdf>.